

Article

Microstructure and Mechanical Properties of Dissimilar Friction Stir Welded AA2024-T4/AA7075-T6 T-Butt Joints

Mohamed M.Z. Ahmed ^{1,2,*} , Mohamed M. El-Sayed Seleman ², Zeinab A. Zidan ², Rashad M. Ramadan ², Sabbah Ataya ^{2,3}  and Naser A. Alsaleh ³

¹ Department of Mechanical Engineering, College of Engineering at Al Kharj, Prince Sattam Bin Abdulaziz University, Al Kharj 11942, Saudi Arabia

² Department of Metallurgical and Materials Engineering, Faculty of Petroleum and Mining Engineering, Suez University, Suez 43512, Egypt; mohamed.elnagar@suezuniv.edu.eg (M.M.E.-S.S.); Eng.zeinab12@yahoo.com (Z.A.Z.); rashadrmn@yahoo.co.uk (R.M.R.); sabbah.ataya@suezuniv.edu.eg (S.A.)

³ Department of Mechanical Engineering, College of Engineering, Al Imam Mohammad Ibn Saud Islamic University, Riyadh 11432, Saudi Arabia; alsaleh@engineer.com

* Correspondence: moh.ahmed@psau.edu.sa; Tel.: +966-011-588-1200

Abstract: Aircraft skin and stringer elements are typically fabricated from 2xxx and 7xxx series high strength aluminum alloys. A single friction stir welding (FSW) pass using a specially designed tool with shoulder/pin diameter ratio (D/d) of 3.20 is used to produce dissimilar T-butt welds between AA2024-T4 and AA7075-T6 aluminum alloys at a constant travel speed of 50 mm/min and different rotational speeds of 400, 600 and 800 rpm. The AA2024-T4 is the skin and the AA7075-T6 is the stringer. Sound joints are produced without macro defects in both the weld top surfaces and the joint corners at all rotational speeds used (400, 600, and 800 rpm). The hardness value of the nugget zone increases by increasing the rotational speed from 150 ± 4 Hv at 400 rpm to 167 ± 3 Hv at 600 rpm, while decreases to reach the as-received AA2024-T4 hardness value (132 ± 3 Hv) at 800 rpm. Joint efficiency along the skin exhibits higher values than that along the stringer. Four morphologies of precipitates were detected in the stir zone (SZ); irregular, almost-spherical, spherical and rod-like. Investigations by electron back scattered diffraction (EBSD) technique showed significant grain refinement in the stir zone of the T-welds compared with the as-received aluminum alloys at 600 rpm due to dynamic recrystallization. The grain size reduction percentages reach 85 and 90 % for AA2024 and AA7075 regions in the mixed zone, respectively. Fracture surfaces along the skin and stringer of T-welds indicate that the joints failed through mixed modes of fracture.

Keywords: dissimilar friction stir welding; AA2024-T4/AA7075-T6Al alloys; t-butt joints; microstructure evaluation; EBSD; fracture surfaces



Citation: Ahmed, M.M.Z.; El-Sayed Seleman, M.M.; Zidan, Z.A.; Ramadan, R.M.; Ataya, S.; Alsaleh, N.A. Microstructure and Mechanical Properties of Dissimilar Friction Stir Welded AA2024-T4/AA7075-T6 T-Butt Joints. *Metals* **2021**, *11*, 128. <https://doi.org/doi:10.3390/met11010128>

Received: 28 December 2020

Accepted: 6 January 2021

Published: 10 January 2021

Publisher's Note: MDPI stays neutral with regard to jurisdictional claims in published maps and institutional affiliations.



Copyright: © 2021 by the authors. Licensee MDPI, Basel, Switzerland. This article is an open access article distributed under the terms and conditions of the Creative Commons Attribution (CC BY) license (<https://creativecommons.org/licenses/by/4.0/>).

1. Introduction

Friction Stir Welding (FSW) is a solid-state welding technique, where similar [1–3] and dissimilar metals [2] are welded without reaching their melting point. FSW has gained significant attention due to its numerous advantages [4–6] over the traditional arc welding methods [7]. However, FSW has also some drawbacks [8–10] which are very little when compared with the traditional welding processes. Various joining configurations in terms of spot [3,11], butt [12–14], corner [15], lap [16–18] and fillet [19] joints have been studied and established for different metals and alloys using FSW technology through optimizing their welding process parameters. However, FSW of high strength to weight ratio aluminum alloys to produce T-joints are still demanding more studies and efforts to evaluate the joint efficiency, and to optimize the welding parameters. Arora et al. [20] reported that the hardness and tensile strength of the friction stir similar butt joint of AA2219 were lower than the base metal. However, a toughness value of the nugget zone enhanced compared to the base metal. Babu et al. [18] studied the effect of pin profiles on the friction stir

welded (FSWed) lap joint quality of the AA2014 aluminum alloy and reported that the strength and the failure mode of joints are related to the hook geometry. Sadeesh et al. [21] studied the influence of using five different tool designs in FSW of dissimilar AA2024 and AA6061 aluminum alloys in butt joints and concluded that the joints efficiency is related to the varying welding process parameters and the shoulder to pin diameter ratio is the main dominant parameter. Manuel et al. [22] investigated the behavior of the friction stir welds of three dissimilar aluminum alloys in a T-joint using three base materials namely, AA2017-T4, AA5083-H111, and AA6082-T6. They reported that the arrangement of the skin materials with respect to the pin rotation direction influence the morphology and the mechanical properties of the joints [22]. In fact, the 2xxx and 7xxx aluminum alloys before FSW were known to be non-weldable by traditional fusion welding processes since number of problems such as porosity, solidification cracks and residual internal stresses are found in the weld. Moreover, the formed dendritic structure during solidification in the fusion zone is significantly deteriorating the mechanical properties of the joints [5].

AA2024 and AA7075 aluminum alloys are typically representing the 2xxx and 7xxx alloys series, respectively, which are usually used intensively to fabricate structural components of automotive and aircraft industries [23–25]. In many applications, especially the aircraft fuselage panels in the form of T-joints; where, the aluminum alloys AA2024 and AA7075 are used as skins and stringers, respectively. The stringer is the stiffening element which reinforces the section of the load carrying skin to avoid buckling and failure. In FSW of T-joints, Cui et al. [26] studied the effect of different rotational speeds on the microstructure and mechanical properties of the T-lap, T-butt-lap, and T-butt joints. They ascribed the formed defects such as tunnel defect, kissing bond, original joint line defect, and zigzag line to the initial matching modes of the blanks, material flow patterns, and insufficient heat input. Acerra et al. [15] investigated the dissimilar AA2024-T4 and AA7075-T6 T-joints and evaluated the design rules for the setup of FSW operations. They concluded that a large shoulder diameter is required to generate a sufficient heat input to fulfill the weld joint. Moreover, the presence of coating layers negatively affects the mechanical properties by a generation of macro and micro defects. In T-butt joints, especially in aerospace industry, the tool pin has been penetrated vertically into the materials setup surface to join three separate parts, two skin parts and vertical stringer element, to produce one-piece T-joint [15].

This work aims to conduct single pass FSW of T-butt joints between AA2024-T4 and AA7075-T6 aluminum alloys as skin and stringer; respectively, at different tool rotational rates of 400, 600 and 800 rpm and a constant welding speed of 50 mm/min. The role of FSW parameters and the welded materials on the microstructure, the strength and the fracture mode will be examined. Attention will be given to investigate the evolved texture using EBSD.

2. Experimental Procedure

Plates of the dissimilar aluminum alloys of AA2024-T4 and AA7075-T6 were friction stir welded in T-butt joints. The dimensions for FSW samples were 4 mm × 50 mm × 200 mm for AA2024-T4 and 5 mm × 100 mm × 200 mm for AA7075-T6 alloys. The T-butt joint setup was designed to be two plates of AA2024-T4 alloy as a skin and one plate of AA7075-T6 as a stringer. The chemical composition of the aluminum alloys was analyzed using Q2 ION-OES -Optical Emission Spectrometry (Bruker, Billerica, MA, USA). The chemical composition of the investigated alloys is listed in Table 1.

Table 1. Chemical analysis (wt. %) of the AA2024-T4 and AA7075-T6 alloys.

Alloy	Elements in wt. %								
	Si	Fe	Cu	Mn	Mg	Cr	Zn	Ti	Al
AA2024-T4	0.20	0.40	3.90	0.40	1.50	0.02	0.17	0.02	Bal
AA7075-T6	0.05	0.22	1.94	0.05	2.66	0.21	5.97	0.01	Bal

The T-butt joints were friction stir welded using gantry type FSW (EG-FSW-M1, made by Suez University, Suez, Egypt) machine [2,6]. Adaptive fixture was designed [15] and fabricated from steel for T-butt joint configuration setup, Figure 1a,b. A constant travel speed of 50 mm/min and three various rotational speeds of 400, 600 and 800 rpm were used in this work. The shoulder tilting angle and the shoulder plunge depth were 3° and 0.20 mm, respectively. The other welding conditions were kept constant. A concave tool shoulder with a diameter of 32 mm and a threaded taper pin with a length of 3.8 mm was used (Figure 1c). The bottom and top diameters of the pin were 12 mm and 10 mm, respectively. The tool was machined from H13 tool steel and heat treated to obtain a hardness value of 58 HRC. Figure 1c shows top view appearance of a friction stir welded joint.

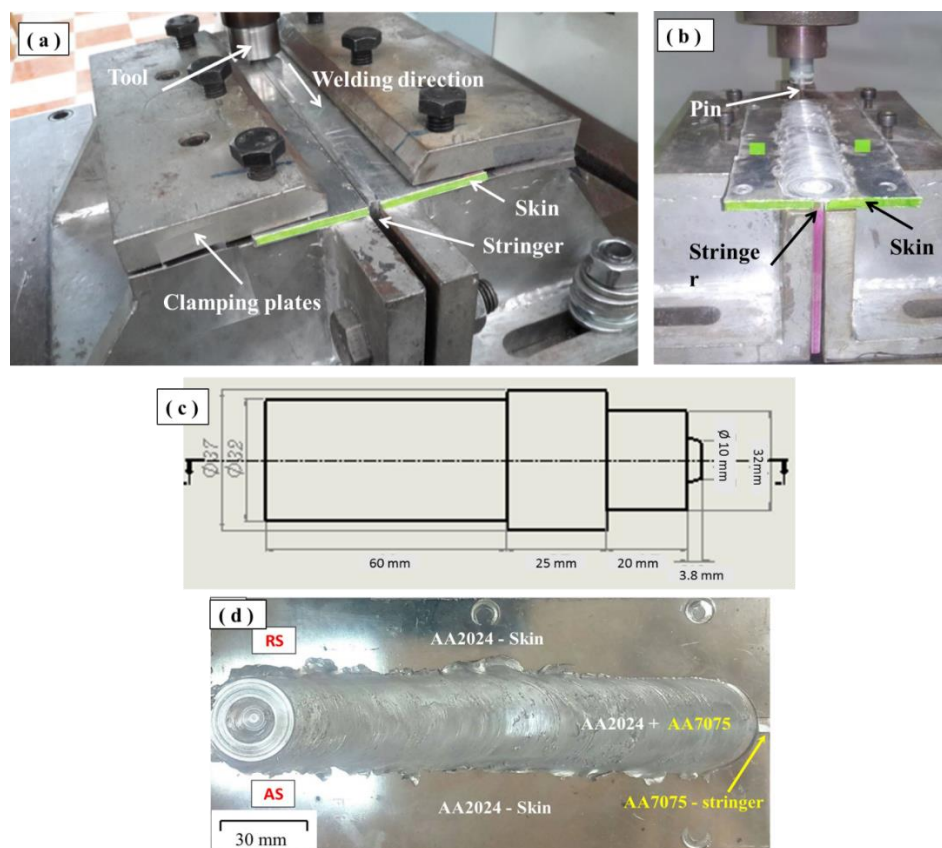


Figure 1. (a,b) FSW fixture setup configuration of AA2024 and AA7075 T-butt joint, (c) Engineering drawing of the used tool (d) top view appearance of a friction stir welded joint.

In order to investigate the developed T-joints microstructure and mechanical properties, the samples were cross-sectioned perpendicular to the welding direction (WD). For microstructural analysis, the sectioned samples were ground using SiC papers with different grit up to 2400 and polished on felt cloth with alumina $0.05 \mu\text{m}$ paste and then etched with Keller's reagent (6 mL hydrofluoric acid, 6 mL hydrochloric acid, 5 mL nitric acid and 150 mL water). Stereo microscope (Optica SZR 10, Optica, Ponteranica (BG), Italy) was used to examine macrostructures of the joints. Microstructural analyses were carried out using optical microscope (OM) Olympus -BX41M-LED, Olympus, Tokyo, Japan. And scanning electron microscopy (SEM) Type Quanta FEG-250 (FEI company, Hillsboro, OR, USA) equipped with electron back scatter diffraction (EBSD) and energy dispersive spectroscopy (EDS) were also used to examine the grain structure, texture and precipitates composition.

Vickers hardness tester machine (HWDV-75, TTS Unlimited, Osaka, Japan) was used to evaluate the hardness profiles along the width of the weld samples using a load of 2.0 kg

and dwell time of 15 s, where the free space between any two indentations was 0.5 mm, which represents at least 2.5 times the maximum indentation diameter. The hardness maps were also analyzed and drawn by collecting three lines measurements across the stir zone (SZ) and the stringer. Two tensile tests were carried out along skin and stringer axes using tensile testing machine (Instron-4208-300 kN capacity, Norwood, MA, USA) at a room temperature and a cross-head speed of 1.0 mm/min, Figures 2 and 3, respectively. At least three tensile samples were prepared from each T-butt joint and the average value of tensile strength was considered. The fracture surfaces of tensile test samples were investigated using the SEM. For EBSD investigation, the polished samples were subjected to electro-polish for 60 sec at $-15\text{ }^{\circ}\text{C}$ and 14 V. The electro-polishing electrolyte consists of 30 vol.% nitric acid in 70 vol.% methanol. EBSD was performed for the base materials (BMs) and stir zone (SZ) of T-butt joints at 20 kV and $0.5\text{ }\mu\text{m}$ step size. The collected EBSD data were analyzed by OIM DC 7.3 software, developed by EDAX, AMETEK, Draper, UT, USA.

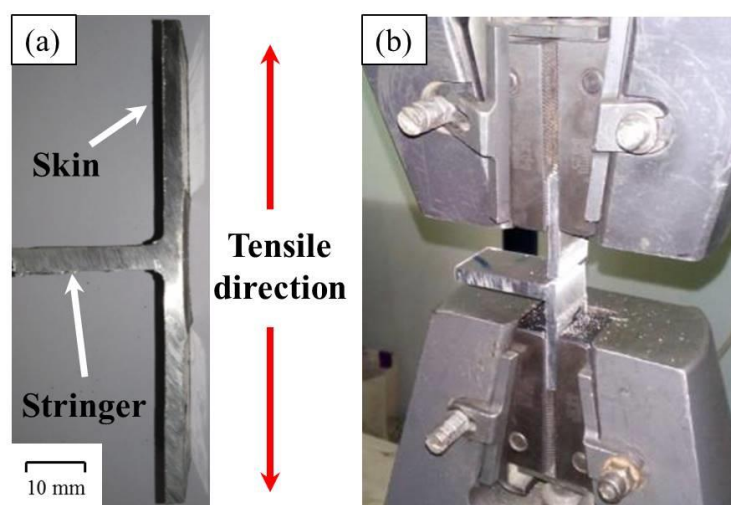


Figure 2. Photographs of tensile testing along skin direction (a) T-butt joint tensile test specimen and (b) after tensile test.

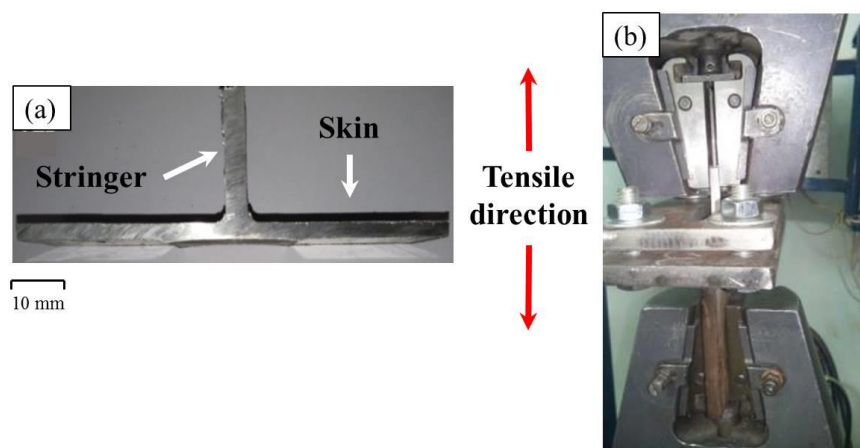


Figure 3. Photographs of tensile testing along stringer direction (a) T-butt joint tensile test specimen and (b) tensile test clamping system.

3. Results and Discussion

3.1. Joint Appearance and Macro-Examinations

Figure 4 shows the appearance of the T-butt joints friction stir welded at different rotational speeds of 400, 600 and 800 rpm. It can be observed that the top surfaces are defect free and also the exit holes are complete with no indications of any tunnel defects.

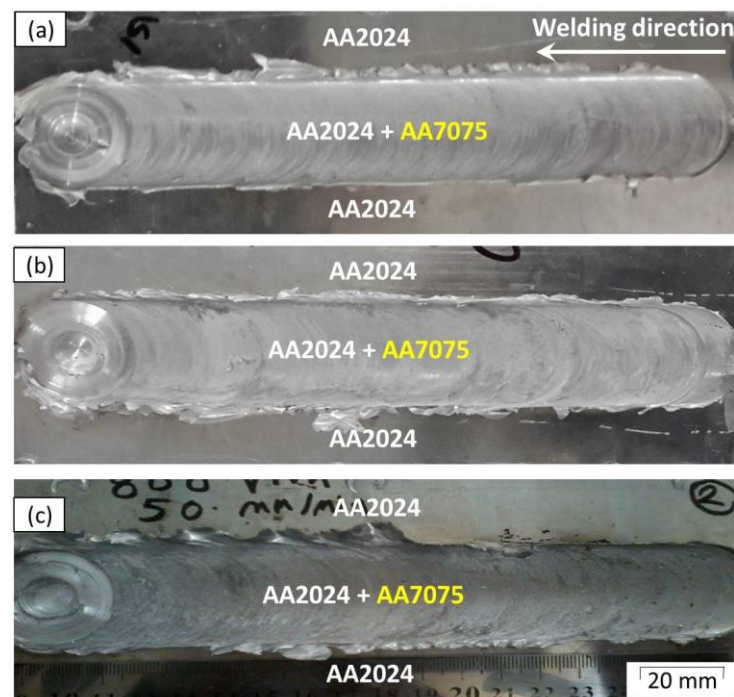


Figure 4. T-butt joint appearance of friction stir welded AA2024 and AA7075 at 50 mm/min welding travel speed and different rotational speeds (a) 400 rpm, (b) 600 rpm, and (c) 800 rpm.

The examination of the cross-section macrostructure of welding zone may be used to clarify the quality of friction stir welded joints. It has been reported that four different zones, namely stir zone (SZ) or nugget zone, thermo-mechanically affected zone (TMAZ), heat affected zone (HAZ) and base material (BM) can be identified in the macrostructure of welds [4]. Several variables like types of BM, thickness of work piece, welding parameters, and tool design play a significant role in the formation of friction stir welded joint features. Actually, the amount of heat input has a great effect on material flow, SZ shape, microstructure grain size and FSW defects. Hence, the quality of joints can be enhanced if the rotation and welding speeds of the FSW process can be carefully controlled. Typical transverse cross-section macrographs of the friction stir welded T-butt-joints of AA2024-T4 and AA7075-T6 are shown in Figure 5. It can be observed that the transverse cross sections showed sound T-butt joints at all the applied FSW parameters. However, the mixing process between the two alloys is significantly enhanced by increasing the rotation speed of the FSW tool such that at the low rotation speed is entirely pertains the whole stringer material (AA7075) within the SZ zone, by increasing the rotation speed the stringer material starts to get dispersed and mixed with the skin material (AA2024). This implies that increasing the rotation speed has resulted in a complex flow pattern that enhanced the two materials mixing and joining.

It is worth mentioning here that the dimensions of the SZ are controlled by the dimensions of the tool shoulder and pin. SZ is usually diffused to be little bit larger than the pin dimensions and has a like-conical form [10]. The widest region is beneath the shoulder diameter, which is ~32 mm and become narrower with the depth to be determined by the pin diameters (12 to 10 mm) and length ($h = 3.8$ mm) as it has been defined in the Figure 5 by the dashed lines.

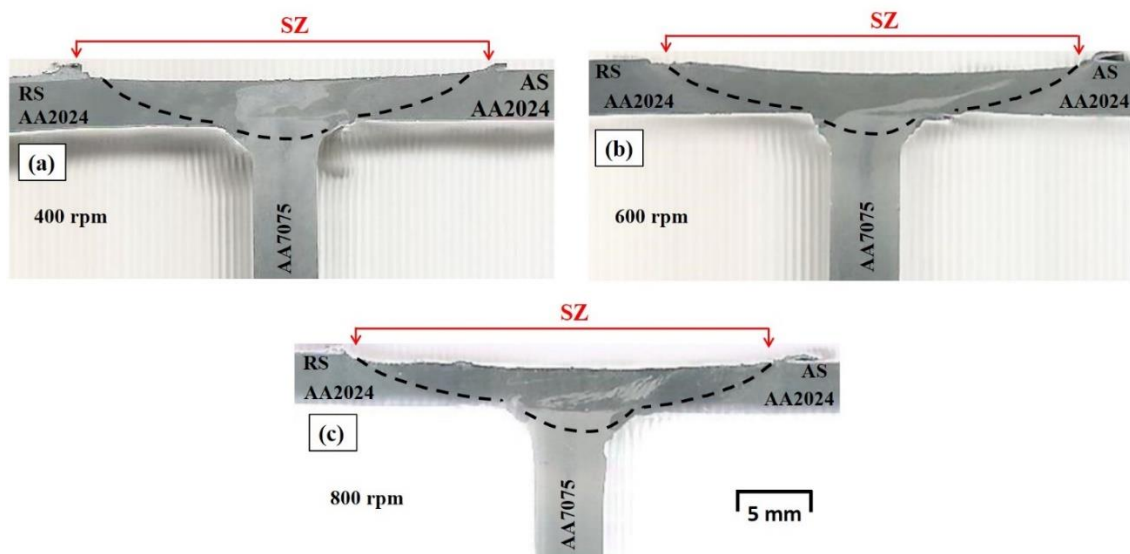


Figure 5. Macrographs of T-butt-joints of friction stir welded AA2024 and AA7075 at different rotational speeds of (a) 400 rpm, (b) 600 rpm, and (c) 800 rpm.

3.2. OM Investigations

Optical microscopy investigations were performed on the transverse cross-sections of the FSWd T-joint specimen's perpendicular to the welding direction. The three zones (SZ, TMAZ, and HAZ) were arranged by SZ from the center line of the weld joint perpendicular to the welding direction in both sides ending HAZ in the BM. The width of each zone and its features are related to the heat input introduced to the work-piece during FSW process, as shown in the joints' macrographs in Figure 5. The variation in heat input in the present work came mainly from the applied different rotational speeds of 400, 600 and 800 rpm where the travel speed is kept constant at 50 mm/min, the heat input index is equal to (ω^2/v) [10]. The microstructures of the cross-sectional dissimilar friction stir welded T-butt joints of AA2024-T4 and AA7075-T6 Al alloys show new formation of the grain structures in the SZ (Figure 6). For friction stir welded T-joint at 400 rpm good mixing between skin and stringer can be clearly seen, as given in Figure 6a. The mixing between skin and stringer in the SZ has improved as the rotation welding speed increased to 600 rpm, Figure 6c. FSW at 600 rpm welding condition converts the initial elongated grains in as AA2024 and AA7075 aluminum alloys to fine equiaxed recrystallized grains in the weld SZ. Moreover, the coarse precipitates given by the lowest rotational speed of 400 rpm become finer and more dispersed. This change in microstructure is ascribed to high temperature and high stirring action by the pin inside skin and stringer which positioned between the two pieces forming the skin (Figure 1a,b). Remarkable coarser grains with very good mixing are observed at the highest rotational speed of 800 rpm, as shown in Figure 6e,f. However, the high heat input presented a chance to generate coarse precipitates in both SZ and TMAZ. Similar results of coarsening the precipitates at such conditions have been noticed in other works [1,27]. It can be concluded that, the best mixing between skin and stringer is obtained at rotational speeds of 600 and 800 rpm. The T-joint produced at 600 rpm rotational speed exhibits finer grains and precipitates in the SZ than the other two joints. Detailed EBSD grain size measurements for the parent alloys and for the friction stir welded material are presented in subchapter 3.5. In the TMAZ no recrystallization is noticed because the frictional heat and plastic deformation are not high enough to cause recrystallization Figure 6b,d,f.

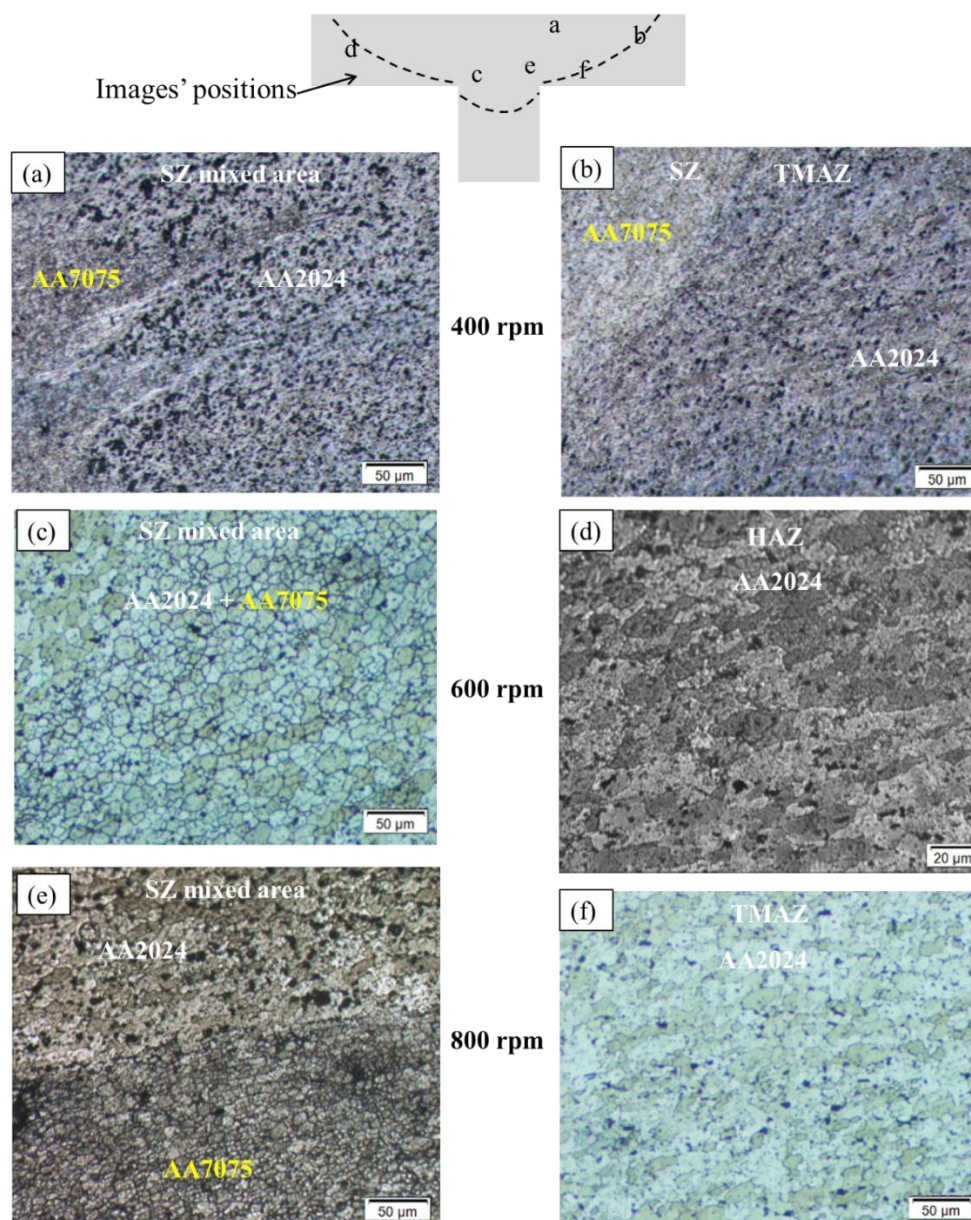


Figure 6. Optical microstructures of AA2024-AA7075 T-butt joint welded at different rotational speeds of (a,b) 400, (c,d) 600 and (e,f) 800 rpm. The positions of the different images are shown in the top schematic drawing.

3.3. Hardness Distribution

The hardness variation along the skin and the stringer of the friction stir welded T-butt joint may give a better prediction about the phenomena involved in this welding process and the causes of loss or increase in strength compared with the base material. The hardness distribution maps of the T-butt joints for all the applied rotational speeds indicate good material mixing at the nugget zone as shown in Figure 7, which is evidence of selecting a proper tool design with shoulder/pin diameter ratio (D/d). The D/d ratio in the current study was 3.20. This ratio agrees well within the value that reported by Saravanan et al. [28] who focused their work on studying the effect of the D/d ratio in the range of 1–4 on the microstructure and mechanical properties of the dissimilar butt-joint of AA2024-T6 and AA7075-T6 Al-alloys. They concluded that the butt joint friction stir welded using a D/d ratio of 3.00 exhibited higher mechanical properties when compared to the other welded joints [28].

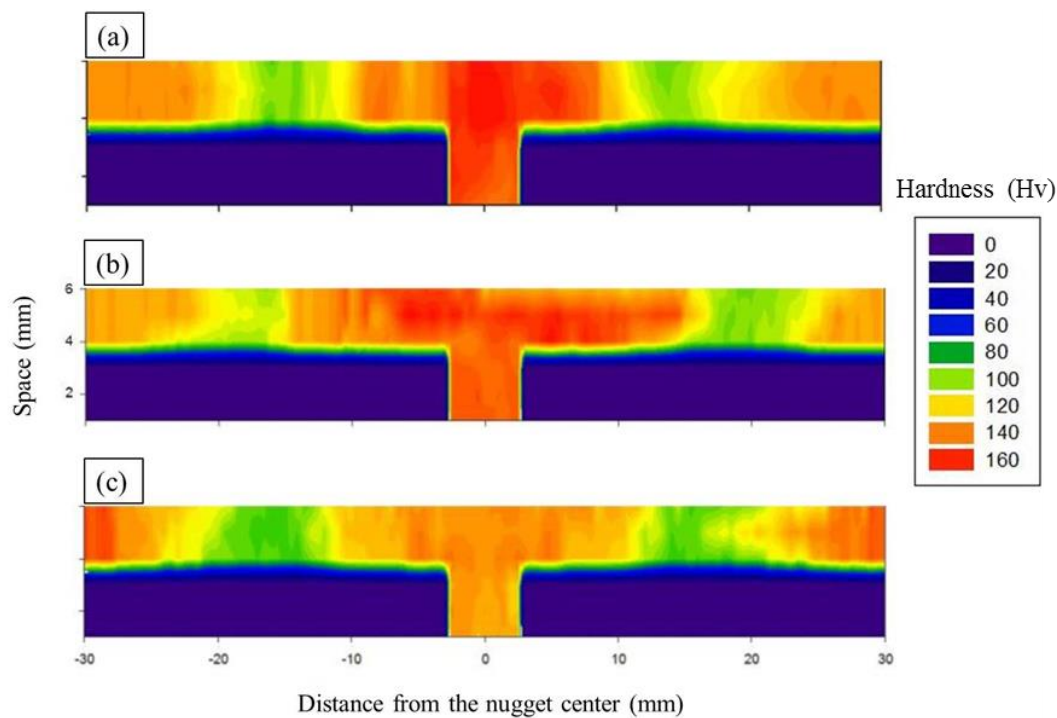


Figure 7. Hardness maps of the T-butt joint AA2024-T4 and AA7075-T6 friction stir welded at different rotational speeds of (a) 400 rpm, (b) 600 rpm and (c) 800 rpm.

The hardness maps show higher hardness at the SZ of the mixed alloys compared to the skin base material AA2024-T4 at the rotational speeds of 400 and 600 rpm, as shown in Figure 7a,b. This increase in the hardness at the SZ can be attributed to two reasons: (i) high proportion of the AA7075-T6 (high hardness alloy) in the SZ and (ii) the finer grain size (dynamically recrystallized) at SZ compared to the base material. According to Hall-Petch relation [29], smaller grain size leads to harder material property. The increasing amount of AA7075-T6 material in the microstructure of the stir zone seems to be also a reason for the higher hardness measured within the nugget zone of the T-butt joint. The highest rotational speed of 800 rpm leads to higher heat generation and slower cooling rate and then causes the formation of relatively coarse grains. And also, leads to the formation coarser precipitates during re-precipitation in the cooling cycle, thus result in lower hardness in the SZ and TMAZ compared to other joints welded at 400 and 600 rpm. The lower hardness observed in the HAZ of both advancing side (AS) and retreating side (RS) of the joints are results of coarsening and dissolution of strengthening precipitates [1–3,13,30]. No obvious differences are seen in the mean values of hardness of HAZ at both the AS and RS of all the welded joints. For the T-joint welded at 800 rpm, a wider softened area evidenced with slightly lower hardness in the SZ as well as in the HAZ of both sides. The slight lower hardness in the SZ and the wider softened region in this joint can be attributed to the high heat input experienced which affects the precipitates coarsening and/or dissolution. The softening behavior at HAZ with a minimum hardness ranging from 98 to 105 Hv is observed. The observed best joint hardness at a rotational speed of 600 rpm which gives proper mixing with adequate generated heat and cooling rate at travel speed of 50 mm/min.

The hardness profile of friction stir welded of heat-treatable AA2024 and AA7075 aluminum alloys depends strongly on the grain size structure, and the precipitates in terms of type, amount, morphology and distribution [4,5]. The difference in grain shape and size of the two base materials is surely important. Furthermore, the amount of solute atoms (Zn, Mg and Cu) of the mixed two materials is also an essential reason of the high hardness in the nugget zone.

3.4. SEM Investigation

As noted by optical examinations of the welded joints (Figure 8) and confirmed with the two modes SEM investigations (Figure 9) the initial coarse elongated grains of the as-received AA2024-T4 and AA7075-T6 base alloys are thermomechanically deformed during FSW and resulted in new recrystallized equiaxed fine grain structures. The microstructures display also fine precipitates decorated the grain boundaries of the fine grains of both AA2024 and AA7075, Figure 8a–f. In addition, coarse and fragmented precipitates are detected in the SZ of the T-joints as given in VCD-mode images Figure 8b,e respectively. Moreover, the friction stir welded AA7075 alloy shows finer recrystallized grain size than that of AA2024 alloy, Figure 8d.

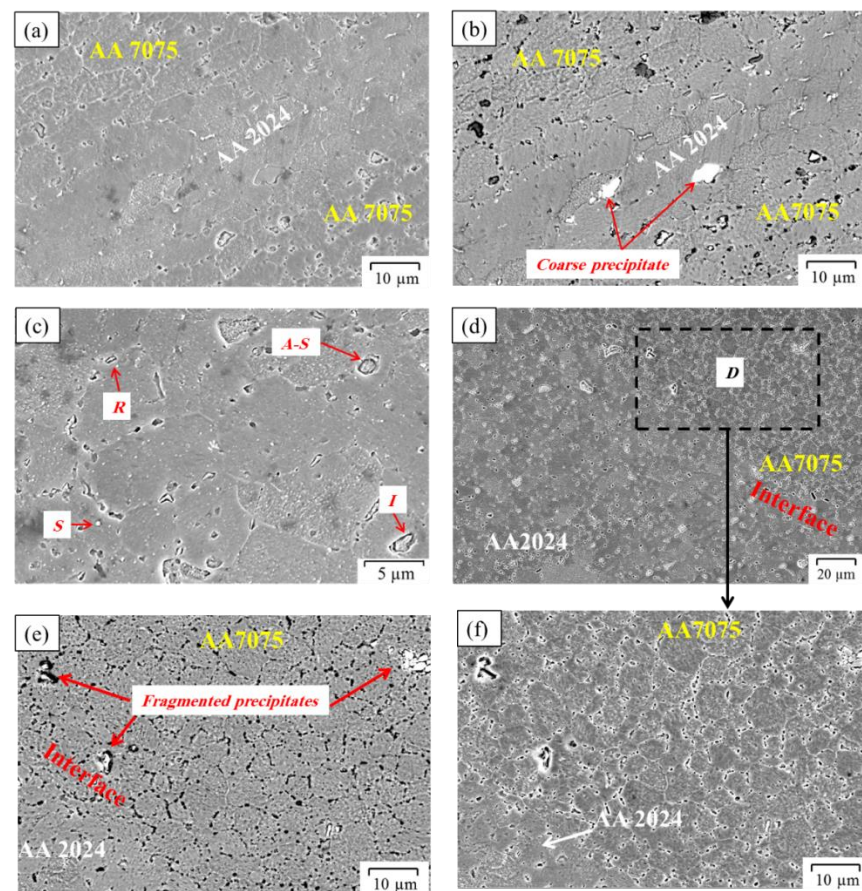


Figure 8. SEM microstructure of Friction stir welded T-joints at different rotational speeds: (a) ETD mode at 400 rpm, (b) in VCD mode, (c) ETD at 600 rpm, (d) low magnification in ETD at 800 rpm, (e) in VCD and (f) high magnification of the selected area (D) in (d).

The FSW and FSP lead to significant change in size and morphology of the precipitates. It can be effectively refined and redistributed both soluble and insoluble particles in precipitation strengthening non-ferrous alloys [31,32]. The precipitates in different regions of FSW zones are strongly function of the local thermo-mechanical cycles. The evolved microstructures in the SZ of the friction stir welded dissimilar T-joints at different rotational speeds are expected to be very complex. In fact, the precipitation phenomena need more research and still out of completely understood [33]. The current study is roughly an important attempt to evaluate morphologies and types of formed precipitates in the SZ of the Friction stir welded T-butt joints of AA2024-T4 and AA7075-T6. This attempt is extended to relate the precipitates influence on the recrystallization process during FSW. The precipitates display four types of morphologies: irregular, almost-spherical, spherical and rod-like and marked by symbols *I*, *A-S*, *S* and *R*, respectively. These morphologies are

shown in the SZ of all the welded joints at the different rotational speeds (400–800 rpm) and typically observed as given for example in Figure 8c.

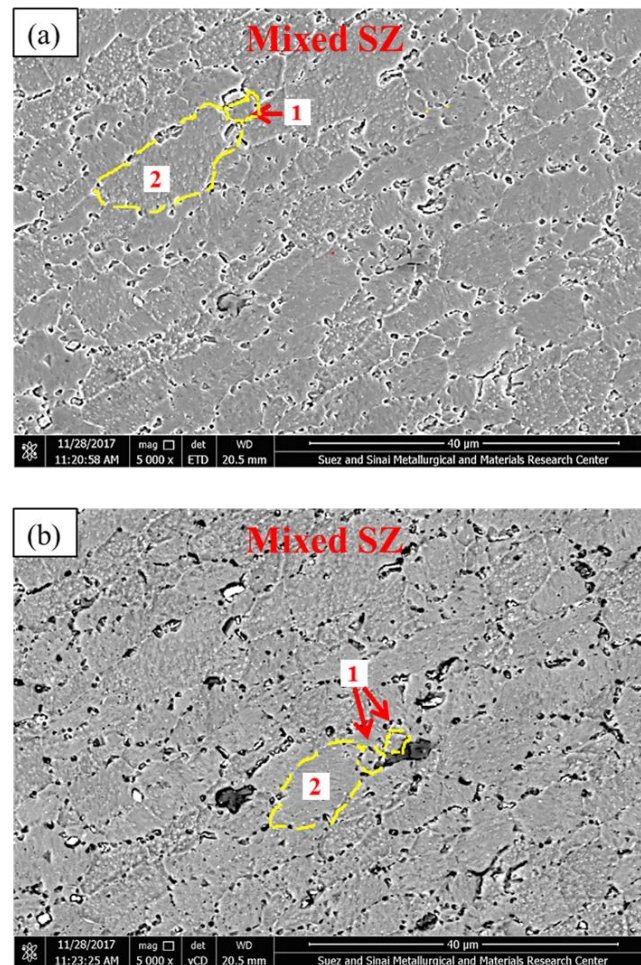


Figure 9. SEM images of T-joint at 400 rpm (a) ETD mode and (b) VCD mode.

Generally, the 2024 and 7075 Al-alloys have unstable nature of precipitates. This means that, the precipitates can coarsen and transformed into more stable precipitates, and/or undergo partial or complete dissolution during suffering high temperatures and may reappear in various morphologies, amounts and crystal structures during cooling.

Precipitates may accelerate or retard the recrystallization process depending on their size and volume fraction. Coarse particles can intensify the driving force of recrystallization and act as nucleation sites, which is known as particle stimulated nucleation (PSN). In contrast, relatively finer particle can retard recrystallization by the particle pinning of the grain boundaries, which is referred to as “Zener Pinning” [34]. Figure 9 shows two examination modes SEM microstructure of Friction stir welded sample at 400 rpm, where location 1 represents fine Dynamically recrystallized (DRX) grains adjacent to coarse particle. However, location 2 denotes coarse DRX grains at a distance from the coarse particles. PSN mechanism is observed to be more effective when the precipitates are present near the grain boundaries rather than within the grain, where the local strain gradient is relatively lower [34,35].

Coarse thermal stable and non-deformable particles interact with moving dislocations producing dislocation piled-ups or loops at the particle-matrix interface, which generates a local strain mismatch at the interface. This local strain field then eases the operation of different slip systems at the interface, which causes the surrounding matrix to rotate to fit the external matrix, creating the so-called particle deformation zone (PDZ) [35,36]. Further

hot deformation, of such PDZs makes them favorable nucleation sites for recrystallization. Due to the high dislocation density in a PDZ, recovery takes place by the formation of new sub-grains, which then increases the misorientation by absorbing more dislocations. When this misorientation achieves from 10 to 15°, a likely recrystallization nuclei has evolved that may then grow into the surrounding matrix [37].

3.5. BM Grain Structure and Texture

For all the welded T-joint, the SZ is mixed regions of AA2024-T4 and AA7075-T6. Degree of mixing enhances as the plasticity of the two Al-alloys increases during the FSW. The plasticity of both alloys is related to the amount of heat input introduced to the work-piece. Actually, plasticity increases as the rotational welding speeds increase at the constant welding parameters. Selected areas of both Al-alloys in the SZ have been analyzed in terms of inverse pole figure (IPF) coloring maps and texture and compared with the as-received features of BMs. Figure 10 shows the IPF coloring maps with respect to the rolling direction (RD) and grain boundary (GB) maps of the BMs (a) AA2024-T4 and (b) AA7075-T6 Al alloys. It can be observed that the BMs are almost similar in terms of grain structure and low angle boundaries (LABs) distributions. The grain shapes are that of the typical rolled materials characterized by large and elongated grains. The GB maps are almost free of LABs, which indicate that both materials were in full-recovered state. The AA2024-T4 Al-alloy showed an average grain size of 47 μm and the AA7075-T6 Al-alloy revealed relatively finer average grain size of 43 μm , as obtained from the grain size distribution histogram shown in Figure 11a,b, respectively. The misorientation angle distribution displays very low density of LABs for the as-received materials, as shown in Figure 11a,b. In terms of texture the 101 and 111 pole figures (PFs) illustrated in Figure 12 fairly shows the rolled texture of the fcc metals although the number of grains obtained in the analyzed areas are limited number.

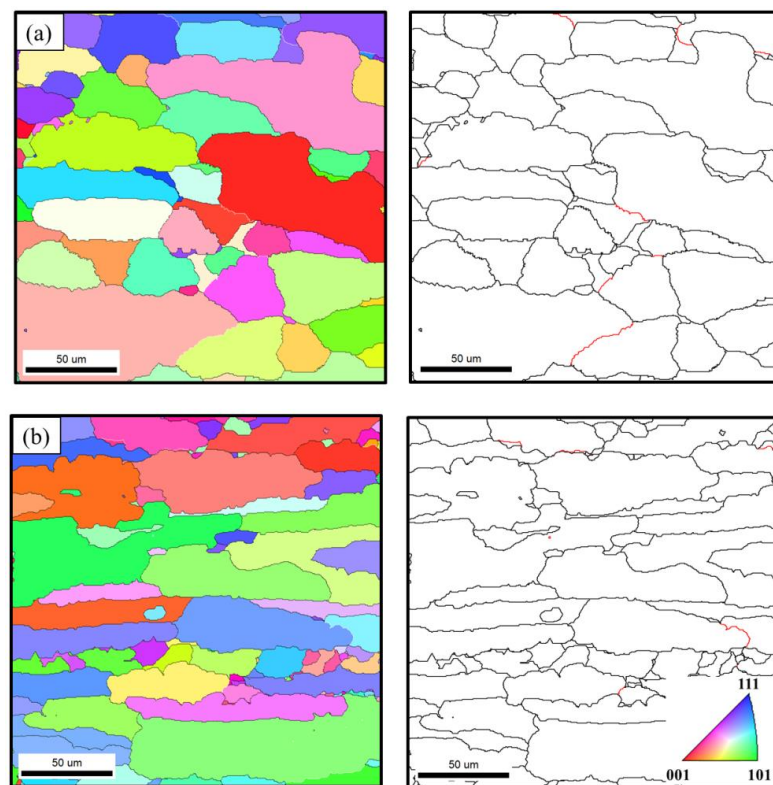


Figure 10. IPF coloring OIM maps relative to rolling direction (RD) and the grain boundary maps with high angle grain boundaries (HAGBs) > 15 in black lines and low angle boundaries (LAGBs) < 15 in red lines, (a) AA2024-T4 and (b) AA7075-T6.

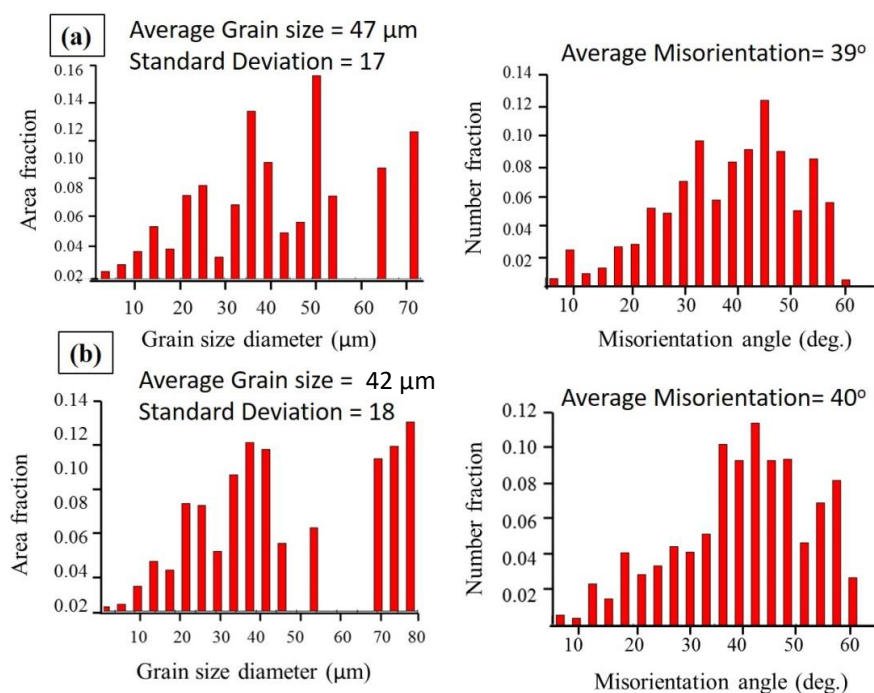


Figure 11. Grain size distribution and misorientation angle distribution of BMs, where (a) AA2024-T4 and (b) AA7075-T6.

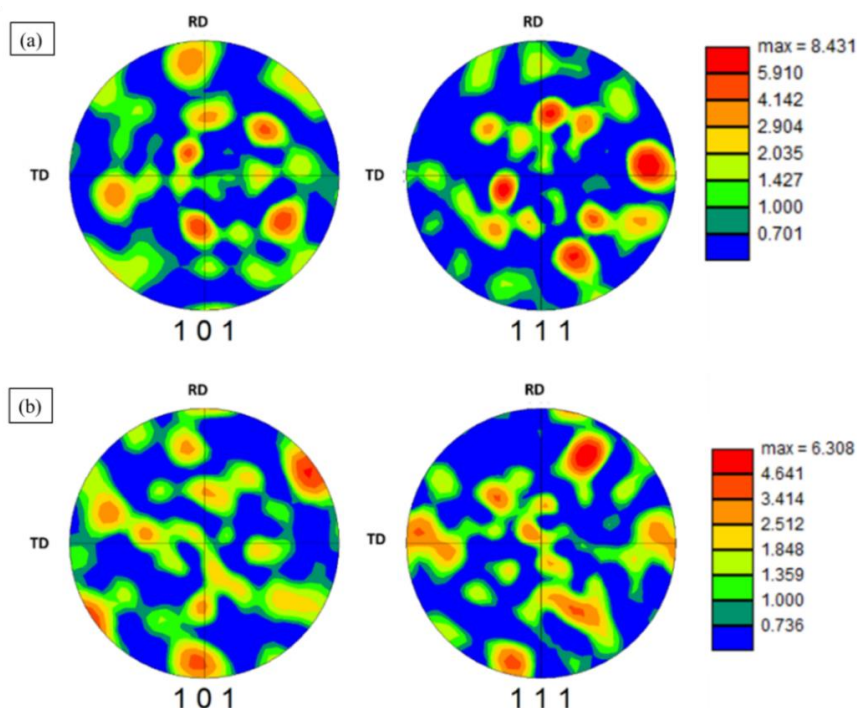


Figure 12. 101 and 111 pole figures (PFs) of BMs, where (a) AA2024-T4 and (b) AA7075-T6.

3.6. Grain Structure and Texture of Friction Stir Welded T-Butt Joints

The SZ of the T-butt joint Friction stir welded AA2024-T4 and AA7075-T6 has been investigated using EBSD by acquiring data at AA2024-T4 and AA7075-T6 regions. The IPF coloring maps with respect to the ND and their corresponding grain boundary maps are presented in Figure 13. It can be observed that the grain structure in both regions is dynamically recrystallized of equiaxed grains. Geometric dynamic recrystallization has

been suggested by number of researchers to be the main recrystallization mechanism in the SZ of the welded aluminum [38,39]. In terms of grain size, it can be noted that in comparison to the BMs it is extremely fine, however a variation in the grain size can be observed between AA2024-T4 and AA7075-T6 regions, Figure 13a,b, respectively. The AA2024-T4 region exhibits coarser grain size relative to the AA7075-T6. The GB maps of the EBSD data obtained from the SZ of the T-butt Friction stir welded joint between AA2024-T4 and AA7075-T6 are presented in Figure 14. The maps are consisted of HAGB $> 15^\circ$ of the major density and a lower density of the LAB ($5\text{--}15^\circ$). The examined SZ areas of AA2024-T4 and AA7075-T6 dominate mainly by HAGBs $> 15^\circ$ with a fraction of 0.801 and 0.924, respectively. While the value of LAGBs $5\text{--}15^\circ$ displays with a fraction of 0.113 and 0.071, respectively.

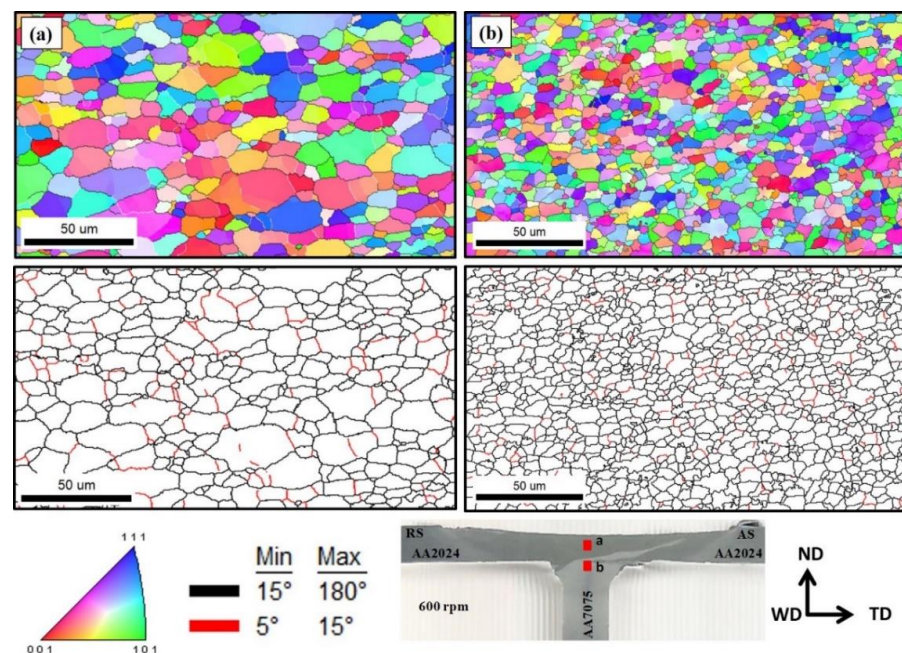


Figure 13. IPF coloring maps and their corresponding grain boundary maps for SZ of T-butt Friction stir welded joint AA2024-T4 and AA7075-T6 produced at 600 rpm, where (a) at AA2024-T4 region and (b) at AA7075-T6 region in the joint produced at 600 rpm. The positions at which the EBSD data collected are indicated with two red rectangles on the macrograph of the joint below the figure. The IPF maps key coloring, grain boundary legend and FSW axes are also presented below the figure.

This data is presented as misorientation angle distribution histogram for the two alloys in Figure 14a,b with the corresponding grain size distribution. The average grain size of the AA2024-T4 is about 11 μm while that of the AA7075-T6 is about 6 μm as given in Figure 14a,b, respectively. This variation can be attributed to the variation in the chemical composition of the two alloys and in consequently to the different types of precipitates in the two alloys. Ahmed et al. [2] in their study of similar and dissimilar Friction stir welded AA7075 and AA5083 reported a variation in the resulted grain size between the AA7075 and the AA5083 inside the same SZ of the dissimilar joints. In terms of the misorientation angle distribution which clearly showing an increase in the LABs density for the data obtained in the AA2024-T4. In terms of texture, the 101 and 111 PFs of this data also calculated and presented in Figure 15a,b. The two alloys show the simple shear texture with only about two times random. This is typical type of texture reported to be obtained in the SZ of the Friction stir welded aluminum alloys [27,40–42]. Crystallographic texture affects the mechanical properties of materials as it expresses the orientation of the crystallographic plans relative to the material reference axes [13]. This directly affects the alignment of the slip systems relative to the axis of the applied load. This why the isotropic materials that of random texture has the same mechanical properties in all direction while in contrast the

anisotropic material that of strong texture its mechanical properties varied based on the direction of the applied load relative to the material reference axes [43–46].

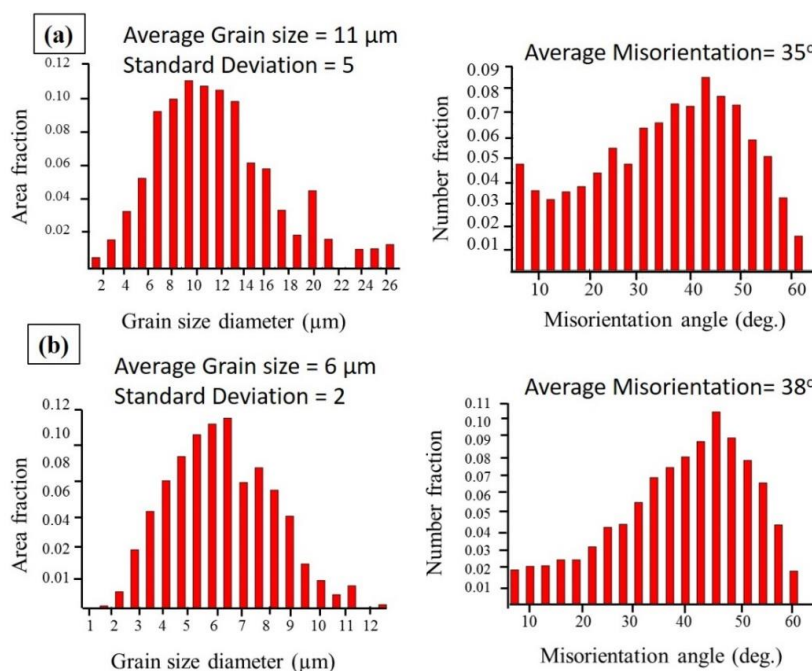


Figure 14. (a) Grain size and misorientation angle distributions of the dissimilar T-butt Friction stir welded joint, where (a) AA2024-T4 region and (b) AA7075-T6 region in the joint produced at 600 rpm.

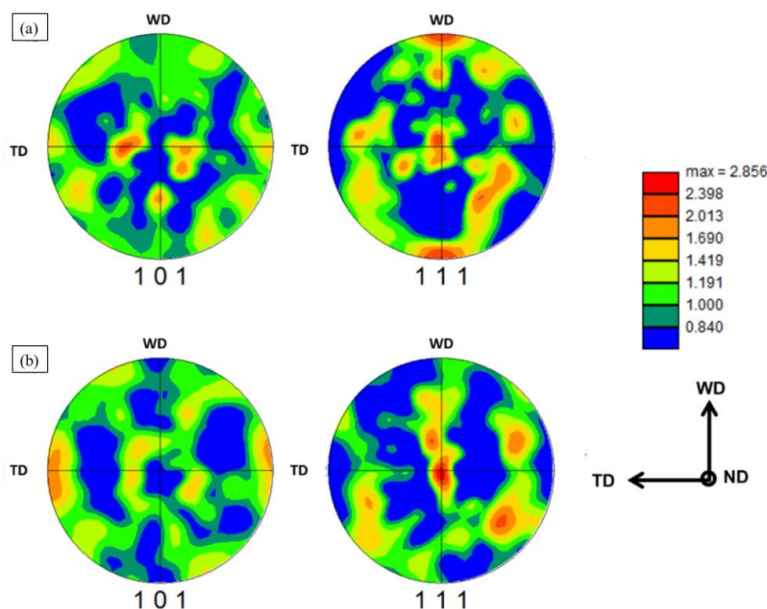


Figure 15. 101 and 111 PFs calculated from the data from SZ of T-butt Friction stir welded joint presented in Figure 13, where (a) AA2024-T4 and (b) AA7075-T6.

3.7. T-Butt Joints Tensile Properties

Figures 16 and 17 show photographs of typical fracture locations of Friction stir welded AA2024-T4 and AA7075-T6 T-butt joints, which were pulled along skin and stringer, respectively. For the welded specimens at 400 rpm pulled along skin (Figure 17a) fracture occurs at the SZ in the RS. This may be attributed to reduction of hardness at the interface

between AA2024-T4 skin and AA7075-T6 stringer (Figure 7a) for the T-joint as a result of insufficient heat input for good mixing in the SZ of the dissimilar aluminum alloys. For 600 rpm, fracture occurs at HAZ region in the RS of AA2024-T4 skin, as shown in Figure 17b. This in agreement with the distribution of the lowest value of hardness in hardness map (Figure 7b) of the joint. For 800 rpm, fracture occurs at TMAZ of RS of the skin, as shown in Figure 17c. This may be ascribed to the lowering hardness map (Figure 7c) in the weld joint as a result of higher heat input.

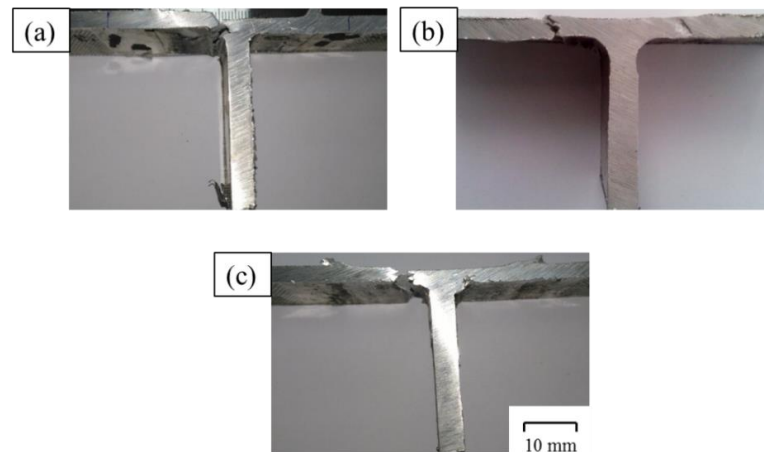


Figure 16. Photographs of fracture locations of T-butt welded specimens along skin. (a) 400 rpm, (b) 600 rpm, and (c) 800 rpm.

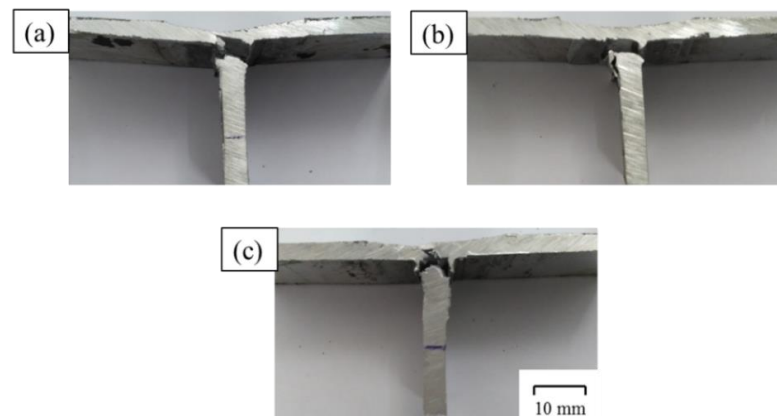


Figure 17. Photographs of fracture locations of T-butt welded specimens along stringer. (a) 400 rpm, (b) 600 rpm, and (c) 800 rpm.

Furthermore, the fracture locations of T-butt welded specimens along stringer are shown in Figure 17. For 400 rpm, Figure 17a, fracture occurs at center of the SZ. It coincides with the variation of hardness values in hardness map (Figure 7a) due to insufficient mixing of AA2024-T4 and AA7075-T6 in the SZ at the lowest rotational speed. For 600 rpm, Figure 17b, the fracture occurs at HAZ in stringer part. It is in good agreement with the lowest hardness values in hardness map (Figure 7b) of stringer AA7075-T6. For 800 rpm, Figure 17c, the fracture occurs at SZ. It coincides with the reduction of hardness values in SZ in hardness map compared to BM AA2024-T4 (Figure 7c).

Joint Efficiency

Joint efficiency of the welded material means the ratio of ultimate tensile strength (UTS) of the joint to the UTS of its base material. It gives an important perception for the joint quality and the mechanical property of the joint. Thus, tensile tests of the produced

T-butt joints were carried out along the skin and stringer directions. Figure 18 shows the joint efficiencies along the skin and stringer of the AA2024 and AA7075 T-butt joints produced using the welding parameters of 400, 600 and 800 rpm rotational speeds, and a constant travel speed of 50 mm/min. For the skin tensile test (perpendicular to welding direction), Figure 18a shows no significant difference in the efficiency values between joints welded at 400 and 600 rpm, while the rotational speed increases from 600 to 800 rpm the efficiency decreases from 83.40 % to reach 72.02 % of the base metal AA2024-T4. Tensile properties in the direction of stringer (perpendicular to welding direction) are given in Figure 18b. It can be seen that the joint efficiencies along stringer increases with increasing tool rotational speeds. The T-butt joints produced at 800 rpm displays the highest joint efficiency of 52.30% of the base metal AA2024-T4. It can be noted from Figure 18a,b, that the joint efficiencies of all produced T-butt joints along the stringer are lower than those of all joints along the skin. This trend is in good agreement with the results obtained by Cui et al. [37] for the similar AA6061-T4 T-butt joints (C-series). Furthermore, they reported that all T-joint efficiencies showed tendency to enhancement with increasing the rotational speeds at constant travel speed.

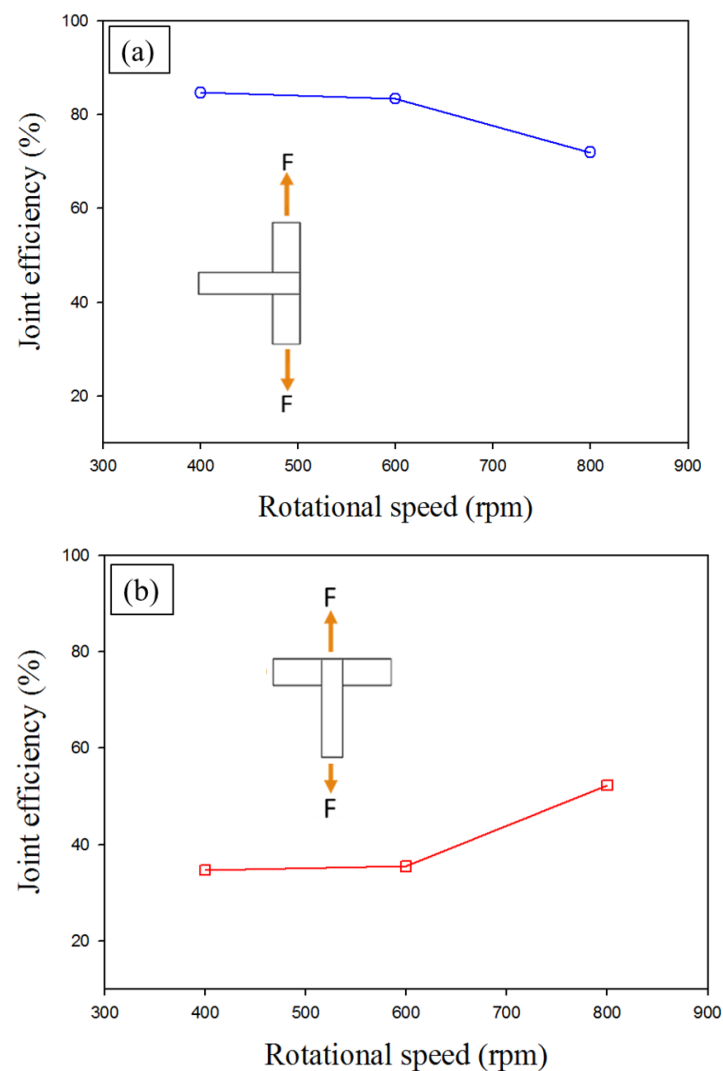


Figure 18. Joint efficiencies against rotational speeds for the T-butt joints of 2024-7075 Al alloys; (a) tensile tested along the skin and (b) along the stringer directions.

It can be noted that for the joint welded at 800 rpm the joint efficiency along the skin direction is the lowest and for the stringer direction is the highest as shown in

Figure 18a,b can be due to two reasons. First, the reduction in the hardness relative to the other two revolution speeds as shown in Figure 7, due to the increased heat input. Second, the reduced skin thickness due to the pressing effect of the shoulder (Figure 5), this is not the case for tension in the stringer direction. Moreover, at 800 rpm the pressing by the shoulder and the increased softening has generated larger fillet than the other two lower rotation speeds (400 and 600 rpm). This large fillet represents more support for the stringer leading to the highest joint efficiency.

The authors are still not satisfied with the attained joint efficiency especially in the skin direction, so that further welding trials should be performed with other welding parameters to overcome the reduction in the skin thickness due to the applied pressure by the tool shoulder.

4. Conclusions

1. Sound T-joints are successfully produced with three plates in T-butt configuration; (two AA2024 plates as skin and one AA7075 plate as stringer) at different rotation speeds and constant traverse speed using FSW tool of large diameter pin of 12 mm to enable one track FSW of the three pieces.
2. All T-butt joint specimens exhibit a W-shaped appearance hardness profiles along the center line of the skin of the welds and reaches the highest level at 600 rpm.
3. Significant grain refining in stir zone of FSW welds is accompanied with dynamic recrystallization compared with the as-received base metals. EDS analyses of the stir zones of the T-joints show four types of precipitates; $Al_6(Mn,Fe,Cu)$, Al_2Cu , Al_2CuMg and Al_7Cu_2Fe .
4. The differences between the AA2024-T4 and AA7075-T6 aluminum alloys in terms of chemical composition, starting grain structure and type of precipitates have strong impact on the recrystallization process, joint efficiency and failure mode of the Friction stir welded T-butt joints.
5. Fracture surfaces along the skin and stringer of all T-welds indicate that the joint failed through mixed modes of fracture, mainly ductile by locally deformed aluminum base and partially brittle via hard phase particles.

Author Contributions: Conceptualization, M.M.Z.A., M.M.E.-S.S., Z.A.Z., and R.M.R.; methodology, Z.A.Z., R.M.R., M.M.Z.A. and M.M.E.-S.S.; validation, S.A., N.A.A. and M.M.Z.A.; formal analysis, S.A. and M.M.Z.A.; investigation, M.M.E.-S.S., S.A. and M.M.Z.A.; writing original draft preparation, M.M.E.-S.S.; M.M.Z.A., R.M.R. and Z.A.Z.; writing—review and editing, S.A., M.M.Z.A. and N.A.A.; project administration, M.M.Z.A., N.A.A. and M.M.E.-S.S. All authors have read and agreed to the published version of the manuscript.

Funding: This research received no external funding.

Institutional Review Board Statement: Not applicable.

Informed Consent Statement: Not applicable.

Data Availability Statement: The data presented in this study are available on request from the corresponding author. The data are not publicly available due to the extremely large size.

Conflicts of Interest: The authors declare no conflict of interest.

References

1. Ahmed, M.M.Z.; Wynne, B.P.; Rainforth, W.M.; Threadgill, P.L. Microstructure, crystallographic texture and mechanical properties of friction stir welded AA2017A. *Mater. Charact.* **2012**, *64*, 107–117. [[CrossRef](#)]
2. Ahmed, M.M.Z.; Ataya, S.; El-Sayed Seleman, M.M.; Ammar, H.R.; Ahmed, E. Friction stir welding of similar and dissimilar AA7075 and AA5083. *J. Mater. Process. Technol.* **2017**, *242*, 77–91. [[CrossRef](#)]
3. Ahmed, M.M.Z.; Ahmed, E.; Hamada, A.S.; Khodir, S.A.; El-Sayed Seleman, M.M.; Wynne, B.P. Microstructure and mechanical properties evolution of friction stir spot welded high-Mn twinning-induced plasticity steel. *Mater. Des.* **2016**, *91*, 378–387. [[CrossRef](#)]
4. Threadgill, P.L. Terminology in friction stir welding. *Sci. Technol. Weld. Join.* **2007**, *12*, 357–360. [[CrossRef](#)]

5. Mishra, R.S.; Ma, Z.Y. Friction stir welding and processing. *Mater. Sci. Eng. R* **2005**, *50*, 1–78. [[CrossRef](#)]
6. Refat, M.; Elashery, A.; Toschi, S.; Ahmed, M.M.Z.; Morri, A.; Mahallawi, I.E.; Ceschini, L. Microstructure, Hardness and Impact Toughness of Heat-Treated Nanodispersed Surface and Friction Stir-Processed Aluminum Alloy AA7075. *Proc. J. Materials Eng. Perform.* **2016**, *25*, 5087–5101. [[CrossRef](#)]
7. Oliveira, J.P.; Barbosa, D.; Fernandes, F.M.B.; Miranda, R.M. Tungsten inert gas (TIG) welding of Ni-rich NiTi plates: Functional behavior. *Smart Mater. Struct.* **2016**, *25*, 03LT01. [[CrossRef](#)]
8. Costa, A.M.S.; Oliveira, J.P.; Pereira, V.F.; Nunes, C.A.; Ramirez, A.J.; Tschiptschin, A.P. Ni-based Mar-M247 superalloy as a friction stir processing tool. *J. Mater. Process. Technol.* **2018**, *262*, 605–614. [[CrossRef](#)]
9. Oliveira, J.P.; Duarte, J.F.; Inácio, P.; Schell, N.; Miranda, R.M.; Santos, T.G. Production of Al/NiTi composites by friction stir welding assisted by electrical current. *Mater. Des.* **2017**, *113*, 311–318. [[CrossRef](#)]
10. Ahmed, M.M.Z.; Ataya, S.; Seleman, M.M.E.; Mahdy, A.M.A.; Alsaleh, N.A.; Ahmed, E. Heat Input and Mechanical Properties Investigation of Friction Stir Welded AA5083/AA5754 and AA5083/AA7020. *Metals (Basel)* **2021**, *68*. [[CrossRef](#)]
11. Boldsaikhan, E.; Fukada, S.; Fujimoto, M.; Kamimuki, K.; Okada, H. Refill friction stir spot welding of surface-treated aerospace aluminum alloys with faying-surface sealant. *J. Manuf. Process.* **2019**, *42*, 113–120. [[CrossRef](#)]
12. Li, S.; Chen, Y.; Zhou, X.; Kang, J.; Huang, Y.; Deng, H. High-strength titanium alloy/steel butt joint produced via friction stir welding. *Mater. Lett.* **2019**, *234*, 155–158. [[CrossRef](#)]
13. Ahmed, M.M.Z.; Wynne, B.P.; Rainforth, W.M.; Addison, A.; Martin, J.P.; Threadgill, P.L. Effect of Tool Geometry and Heat Input on the Hardness, Grain Structure, and Crystallographic Texture of Thick-Section Friction Stir-Welded Aluminium. *Metall. Mater. Trans. A* **2019**, *50*, 271–284. [[CrossRef](#)]
14. Ahmed, M.M.Z.; Wynne, B.P.; Martin, J.P. Effect of friction stir welding speed on mechanical properties and microstructure of nickel based super alloy Inconel 718. *Sci. Technol. Weld. Join.* **2013**, *18*, 680–687. [[CrossRef](#)]
15. Acerra, F.; Buffa, G.; Fratini, L.; Troiano, G. On the FSW of AA2024-T4 and AA7075-T6 T-joints: An industrial case study. *Int. J. Adv. Manuf. Technol.* **2010**, *48*, 1149–1157. [[CrossRef](#)]
16. Shinoda, T.; Suzuki, J. Observation of metal flow phenomenon of lap joints during friction stir welding. *Mater. Sci. Forum* **2004**, *449–452*, 421–424. [[CrossRef](#)]
17. Argade, G.R.; Shukla, S.; Liu, K.; Mishra, R.S. Friction stir lap welding of stainless steel and plain carbon steel to enhance corrosion properties. *J. Mater. Process. Technol.* **2018**, *259*, 259–269. [[CrossRef](#)]
18. Babu, S.; Janaki Ram, G.D.; Venkitakrishnan, P.V.; Reddy, G.M.; Rao, K.P. Microstructure and Mechanical Properties of Friction Stir Lap Welded Aluminum Alloy AA2014. *J. Mater. Sci. Technol.* **2012**, *28*, 414–426. [[CrossRef](#)]
19. Scialpi, A.; De Filippis, L.A.C.; Cavaliere, P. 39-Influence of shoulder geometry on microstructure and mechanical properties of friction stir welded 6082 aluminium alloy. *Mater. Des.* **2007**, *28*, 1124–1129. [[CrossRef](#)]
20. Arora, K.S.; Pandey, S.; Schaper, M.; Kumar, R. Microstructure Evolution during Friction Stir Welding of Aluminum Alloy AA2219. *J. Mater. Sci. Technol.* **2010**, *26*, 747–753. [[CrossRef](#)]
21. Sadeesh, P.; M, V.K.; Rajkumar, V.; Avinash, P.; Arivazhagan, N.; Ramkumar, K.; Narayanan, S. Studies on friction stir welding of AA 2024 and AA 6061 dissimilar metals. *Procedia Eng.* **2014**, *75*, 145–149. [[CrossRef](#)]
22. Manuel, N.; Galv, I.; Leal, R.M.; Costa, J.D. Nugget Formation and Mechanical Behaviour of Friction Stir Welds of Three Dissimilar Aluminum Alloys. *Materials* **2020**, *13*, 2664. [[CrossRef](#)] [[PubMed](#)]
23. Dursun, T.; Soutis, C. Recent developments in advanced aircraft aluminium alloys. *Mater. Des.* **2014**, *56*, 862–871. [[CrossRef](#)]
24. Tavares, S.M.O.; dos Santos, J.F.; de Castro, P.M.S.T. Friction stir welded joints of Al-Li Alloys for aeronautical applications: Butt-joints and tailor welded blanks. *Theor. Appl. Fract. Mech.* **2013**, *65*, 8–13. [[CrossRef](#)]
25. Dubourg, L.; Merati, A.; Gallant, M.; Jahazi, M. Manufacturing of aircraft panels by friction stir lap welding of 7075-T6 stringers on 2024-T3 skin: Process optimisation and mechanical properties. In Proceedings of the 7th International Friction Stir Welding Symposium; TWI: Osaka, Japan, 2008.
26. Cui, L.; Yang, X.; Zhou, G.; Xu, X.; Shen, Z. Characteristics of defects and tensile behaviors on friction stir welded AA6061-T4. *Mater. Sci. Eng. A* **2012**, *543*, 58–68. [[CrossRef](#)]
27. Ahmed, M.M.Z.; Wynne, B.P.; El-Sayed Seleman, M.M.; Rainforth, W.M. A comparison of crystallographic texture and grain structure development in aluminum generated by friction stir welding and high strain torsion. *Mater. Des.* **2016**, *103*, 259–267. [[CrossRef](#)]
28. Saravanan, V.; Rajakumar, S.; Banerjee, N.; Amuthakkannan, R. Effect of shoulder diameter to pin diameter ratio on microstructure and mechanical properties of dissimilar friction stir welded AA2024-T6 and AA7075-T6 aluminum alloy joints. *Int. J. Adv. Manuf. Technol.* **2016**, *3637–3645*. [[CrossRef](#)]
29. Hansen, N. Hall—Petch relation and boundary strengthening. *Scr. Mater.* **2004**, *51*, 801–806. [[CrossRef](#)]
30. Ahmed, M.M.Z.; Wynne, B.P. Post Weld Heat Treatment of Friction Stir Welded AA2017. In *Proceedings of the Light Metals 2012*; TMS: Warrendale, PA, USA; pp. 12–14. [[CrossRef](#)]
31. Pasebani, S.; Charit, I.; Mishra, R.S. Effect of tool rotation rate on constituent particles in a friction stir processed 2024Al alloy. *Mater. Lett.* **2015**, *160*, 64–67. [[CrossRef](#)]
32. Palanivel, S.; Arora, A.; Doherty, K.J.; Mishra, R.S. A framework for shear driven dissolution of thermally stable particles during friction stir welding and processing. *Mater. Sci. Eng. A* **2016**, *678*, 308–314. [[CrossRef](#)]

33. Su, J.-Q.; Nelson, T.; Mishra, R.; Mahoney, M. Microstructural investigation of friction stir welded 7050-T651 aluminium. *Acta Mater.* **2003**, *51*, 713–729. [[CrossRef](#)]
34. Schlegel, S.M.; Hopkins, S.; Frary, M. Effect of grain boundary engineering on microstructural stability during annealing. *Scr. Mater.* **2009**, *61*, 88–91. [[CrossRef](#)]
35. Tangen, S.; Sjølstad, K.; Furu, T.; Nes, E. Effect of Concurrent Precipitation on Recrystallization and Evolution of the P-Texture Component in a Commercial Al-Mn Alloy. *Metall. Mater. Trans. A* **2010**, *41*, 2970–2983. [[CrossRef](#)]
36. Robson, J.D.; Henry, D.T.; Davis, B. Particle effects on recrystallization in magnesium—manganese alloys: Particle-stimulated nucleation. *Acta Mater.* **2009**, *57*, 2739–2747. [[CrossRef](#)]
37. Cai, B.; Adams, B.L.; Nelson, T.W. Relation between precipitate-free zone width and grain boundary type in Relation between precipitate-free zone width and grain boundary type in 7075-T7 Al alloy. *Acta Mater.* **2007**, *55*, 1543–1553. [[CrossRef](#)]
38. Mcnelley, T.R.; Swaminathan, S.; Su, J.Q. Recrystallization mechanisms during friction stir welding / processing of aluminum alloys. *Scr. Mater.* **2008**, *58*, 349–354. [[CrossRef](#)]
39. Etter, A.L.; Baudin, T.; Fredj, N.; Penelle, R. Recrystallization mechanisms in 5251 H14 and 5251 O aluminum friction stir welds. *Mater. Sci. Eng. A* **2007**, *445–446*, 94–99. [[CrossRef](#)]
40. Ahmed, M.Z.; Wynne, B.P.; Rainforth, W.M.; Martin, J.P. Crystallographic Texture Investigation of Thick Section Friction Stir Welded AA6082 and AA5083 Using EBSD. *Key Eng. Mater.* **2018**, *786*, 44–51. [[CrossRef](#)]
41. Ahmed, M.M.Z.; Wynne, B.P.; Rainforth, W.M.; Threadgill, P.L. Quantifying crystallographic texture in the probe-dominated region of thick-section friction-stir-welded aluminium. *Scr. Mater.* **2008**, *59*, 507–510. [[CrossRef](#)]
42. Ahmed, M.M.Z.; Wynne, B.P.; Rainforth, W.M.; Threadgill, P.L. Through-thickness crystallographic texture of stationary shoulder friction stir welded aluminium. *Scr. Mater.* **2011**, *64*, 45–48. [[CrossRef](#)]
43. Divinski, S.V.; Dnieprenko, V.N. Texture contribution to the anisotropy of physical properties. *J. Phys. Condens. Matter* **1994**, *6*, 8503–8512. [[CrossRef](#)]
44. Fouad, D.M.; El-Garaihy, W.H.; Ahmed, M.M.Z.; El-Sayed Seleman, M.M.; Salem, H.G. Influence of multi-channel spiral twist extrusion (MCSTE) processing on structural evolution, crystallographic texture and mechanical properties of AA1100. *Mater. Sci. Eng. A* **2018**, *737*, 166–175. [[CrossRef](#)]
45. Randle, V. Application of electron backscatter diffraction to grain boundary characterisation. *Int. Mater. Rev.* **2004**, *49*, 1–11. [[CrossRef](#)]
46. Rollett, A.D. Crystallographic Texture Change during Grain Growth. *JOM* **2004**, *56*, 63–68. [[CrossRef](#)]